Pressure dependence of ferromagnetic phase boundary in BaVSe₃ studied with high-pressure μ^+SR

Jun Sugiyama ®,[1,2,3,*] Wataru Higemoto,[2] Daniel Andreica,[4] Ola Kenji Forslund,[5] Elisabetta Nocerino,[5] Martin Månsson ®,[5] Yasmine Sassa,[6] Ritu Gupta ®,[7] Rustem Khasanov ®,[7] Hiroto Ohta,[8] and Hiroyuki Nakamura[8]

[1]*Neutron Science and Technology Center, Comprehensive Research Organization for Science and Society (CROSS), Tokai, Ibaraki 319-1106, Japan*
[2]*Advanced Science Research Center, Japan Atomic Energy Agency, Tokai, Ibaraki 319-1195, Japan*
[3]*High Energy Accelerator Research Organization (KEK), Tokai, Ibaraki 319-1106, Japan*
[4]*Faculty of Physics, Babes-Bolyai University, 400084, Cluj-Napoca, Romania*
[5]*Department of Applied Physics, KTH Royal Institute of Technology, Roslagstullsbacken 21, SE-106 91 Stockholm, Sweden*
[6]*Department of Physics, Chalmers University of Technology, SE-412 96 Göteborg Sweden*
[7]*Laboratory for Muon Spin Spectroscopy, Paul Scherrer Institute, CH-5232, Villigen, PSI, Switzerland*
[8]*Department of Materials Science and Engineering, Kyoto University, Kyoto 606-8501, Japan*

The magnetic nature of a quasi-one-dimensional compound, BaVSe₃, has been investigated with positive muon spin rotation and relaxation (μ^+SR) measurements at ambient and high pressures. At ambient pressure, the μ^+SR spectrum recorded under zero external magnetic field exhibited a clear oscillation below the Curie temperature ($T_C \sim 41$ K) due to the formation of quasistatic ferromagnetic order. The oscillation consisted of two different muon spin precession signals, indicating the presence of two magnetically different muon sites in the lattice. However, the two precession frequencies, which correspond to the internal magnetic fields at the two muon sites, could not be adequately explained with relatively simple ferromagnetic structures using the muon sites predicted by density functional theory calculations. The detailed analysis of the internal magnetic field suggested that the V moments align ferromagnetically along the c axis but slightly canted toward the a axis by 28° that is coupled antiferromagnetically. The ordered V moment (M_V) is estimated as (0.59, 0, 1.11) μ_B. As pressure increased from ambient pressure, T_C was found to decrease slightly up to about 1.5 GPa, at which point T_C started to increase rapidly with the further increase of the pressure. Based on a strong ferromagnetic interaction along the c axis, the high-pressure μ^+SR result revealed that there are two magnetic interactions in the ab plane; one is an antiferromagnetic interaction that is enhanced with pressure, mainly at pressures below 1.5 GPa, while the other is a ferromagnetic interaction that becomes predominant at pressures above 1.5 GPa.

I. INTRODUCTION

In the quasi-one-dimensional (Q1D) triangular compounds, in which the 1D ferromagnetic (FM) interaction along the c axis is stronger than the two-dimensional (2D) FM and/or antiferromagnetic (AF) interactions in the ab plane, the magnetic ground state is naturally determined by the competition between the 2D-FM and 2D-AF interactions. When the 1D FM chains form a 2D triangular lattice (2DTL) with $S = \frac{1}{2}$, geometrical frustration provides further complexity in determining the magnetic ground state [1]. Since the delicate balance of the multiple 2D interactions in such a Q1D-2DTL system is expected to be affected by tuning the interchain distances with pressure, the magnetic phases could also

drastically depend on pressure. To study the magnetic nature of the Q1D-2DTL system, a positive muon spin rotation and relaxation (μ^+SR) experiment was initiated, since μ^+SR is one of the most powerful tools for studying internal magnetic fields in solids at both ambient and high pressures due to its unique spatial and time resolutions [2,3]. In fact, the recent ambient and high-pressure μ^+SR work on a Q1D-2DTL compound, BaVS₃ [4], which is known to exhibit a metal-insulator transition at $T_{MI} = 70$ K driven by the formation of a commensurate charge density wave (CDW) Peierls ground state [5–10], has clarified that BaVS₃ enters a linear incommensurate spin density wave ordered state below the Néel temperature (T_N) 31 K at ambient pressure [4,11]. Furthermore, T_N is almost constant as the pressure (p) increases from ambient pressure to 1.4 GPa, then T_N decreases rapidly for $p > 1.4$ GPa, and finally disappears at $p \sim 1.8$ GPa [4], above which a metallic phase is stabilized, Hence, combining the pressure dependence of T_{MI} [12–15], T_N is found to coincide with T_{MI} at $p > 1.4$ GPa [4].

Despite a glamorous electronic and magnetic phase diagram in BaVS₃, there are a limited number of experiments on the isostructural compound BaVSe₃ [17–22]. BaVSe₃

*juns@triumf.ca or j_sugiyama@cross.or.jp
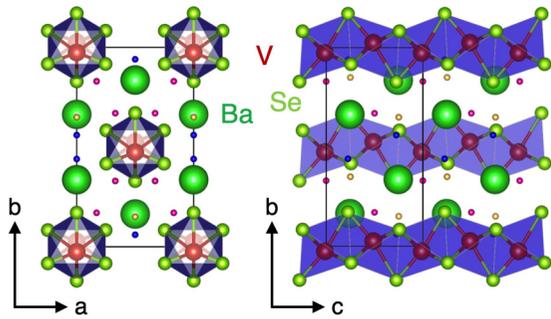
FIG. 1. Crystal structure of orthorhombic $BaVSe_3$ with space group $Cmc2_a$ drawn with VESTA [16]. Lattice parameters are $a = 6.992(2)$Å, $b = 12.113(3)$Å, and $c = 5.859(1)$Å [17]. Large green spheres represent Ba, orange medium spheres represent V, and light green medium-small spheres represent Se. Due to the displacement of V ions along the b axis, the one-dimensional (1D) V chain along the c axis is no longer linear but zigzag in the orthorhombic phase. The three muon sites predicted by density functional theory (DFT) calculations are drawn with small yellow, blue, and pink spheres at $\mu 1$ (0, 0.35, 0.25), $\mu 2$ (0, 0.44, 0.225), and $\mu 3$ (0.33, 0.33, 0), respectively.

undergoes a structural phase transition from a high-temperature hexagonal phase with space group $P6_3/mmc$ to a low-temperature orthorhombic phase with space group $Cmc2_a$ at $T_s = 310$ K [17,18] (Fig. 1). $BaVSe_3$ exhibits a paramagnetic metallic behavior at high temperatures and enters an FM metallic phase below the Curie temperature (T_C) at 43 K [18,19]. Magnetization and torque measurements on a single crystal sample revealed that the easy magnetization axis in the FM phase is parallel to the chain direction, i.e., the c axis [20], as expected. Recent electrical resistivity (ρ) measurements performed under pressure on a single crystal suggested that T_C slightly but monotonically increases with pressure up to 2.8 GPa, based on the change in slope of the $\rho(T)$ curve ($d\rho/dT$) at T_C [21]: that is, $T_C \sim 45$ K at $p = 2.8$ GPa. This would imply that the balance of the two interactions in $BaVSe_3$ is already shifted to the FM side even at ambient pressure.

To confirm the FM spin structure and the pressure dependence of T_C, one needs to study the magnetic nature of $BaVSe_3$ with a direct microscopic magnetic measurement technique under ambient and high pressures, such as neutron diffraction, vanadium nuclear magnetic resonance (V-NMR), and/or μ^+SR. Following upon the high-pressure μ^+SR work on $BaVS_3$ [4], we report here the pressure dependence of the FM phase boundary in $BaVSe_3$ determined with μ^+SR and demonstrate the presence of a competition between the AF and FM interactions in $BaVSe_3$.

II. EXPERIMENTAL

A powder sample of $BaVSe_3$ was prepared by a conventional solid state reaction technique reported in Ref. [19]. A mixture of BaSe, VSe_2, and Se with a molar ratio of 1:1:0.1 was heated in an evacuated quartz tube at 1223 K for 100 h. The sample was characterized by powder x-ray diffraction analysis and magnetization measurements with a superconducting quantum interference device magnetometer (MPMS, Quantum Design), as seen in Fig. 2.
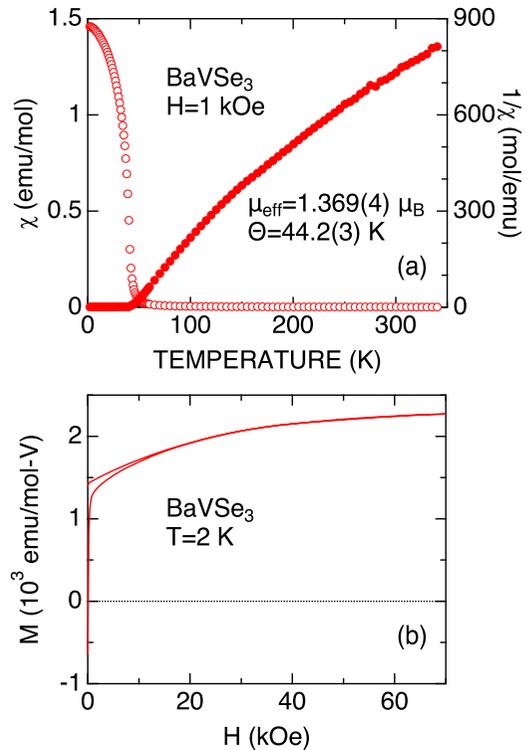
FIG. 2. (a) The temperature dependencies of magnetic susceptibility ($\chi = M/H$) and inverse susceptibility ($1/\chi = H/M$) recorded under the magnetic field $H = 1$ kOe and (b) the relationship between magnetization (M) and magnetic field (H) recorded at 2 K for $BaVSe_3$. In (a), blue solid lines represent the best fit using a Curie-Weiss law, $\chi = \chi_0 + C/(T - \Theta)$, in the temperature range between 50 and 340 K. Such a fit provides that $C = 0.2346(14)$ emuK/mol-Co and $\Theta = 44.2(3)$ K, leading to $\mu_{eff} = 1.369(4) \mu_B/V$. These values are comparable to the values in Refs. [19–21].

The μ^+SR spectra of $BaVSe_3$ were recorded using both the General Purpose Spectrometer (GPS) at the surface muon beamline piM3 and the General Purpose Decay-Channel Spectrometer (GPD) at the decay beamline μE1 of the Laboratory for Muon Spin Spectroscopy (LMU) of the Paul Scherrer Institute (PSI) in Switzerland. On GPS, approximately 200 mg of powder sample was placed in an envelope with 1×1 cm^2 area, made of Al-coated Mylar tape with 0.05 mm thickness to minimize the signal from the envelope. The envelope was attached to a fork-type low-background sample holder and inserted in a liquid-He flow-type cryostat for measurements in the temperature range between 1.6 and 70 K.

On GPD, three pelletized discs of the powder sample with 6 mm diameter and 15 mm total height (5 mm each) were stacked in a piston-cylinder-type pressure cell made of MP35N alloy. To apply hydrostatic pressure to the sample, Daphne oil was used as a pressure transmitting medium. The actual pressure at low temperatures was estimated by measuring the superconducting transition temperature of an indium wire placed at the bottom of the sample space, by alternating current susceptibility. The accuracy of the pressure determined by such a measurement is estimated as ±0.01 GPa

[23]. A Janis ^{4}He flow cryostat was used to reach temperatures as low as 2 K.

The μ^+SR time spectra were recorded at temperatures between 1.6 and 70 K under zero field (ZF) and externally applied magnetic field, namely, weak transverse field (wTF) and longitudinal field (LF). Here, TF [LF] means the field applied perpendicular [parallel] to the initial μ^+ spin polarization, and "weak" means that the field is very small (50 Oe, this time) compared with the internal FM field. The experimental techniques are described in more detail elsewhere [2,3,24,25]. The obtained μ^+SR data were analyzed with the MUSRFIT software suite [26].

The muon sites and local spin density at each muon site in the BaVSe$_3$ lattice were predicted by density functional theory (DFT) calculations using a full-potential linearized augmented plane-wave method within generalized gradient approximations as implemented in WIEN2k program package [27]. In the calculations, the lattice parameters and atomic positions of BaVSe$_3$ were taken from Ref. [22]. The magnetic moments were aligned parallel to the c axis through spin-orbit coupling. The muffin tin potential radii (R_{MT}) for Ba, V, and Se were taken to be 1.32, 1.20, and 1.06 Å, respectively. The energy cutoff was chosen to be $R_{MT} \times K_{max} = 7.0$, and $11 \times 11 \times 11$ k-points meshes were used in the Brillouin zone. Here, K_{max} is the maximum modulus for the reciprocal vectors. Such predictions reveal that there are three possible muon sites in the lattice: (0, 0.35, 0.25), (0, 0.44, 0.225), and (0.33, 0.33, 0) (see Fig. 1), defined according to the local Coulomb potential minima.

III. RESULTS

A. wTF-μ^+SR at ambient pressure

To confirm the sample quality and determine T_C and the transition width (δT_C), the μ^+SR spectrum was measured in a wTF. Figure 3(a) shows wTF-μ^+SR spectra recorded below and above T_C. The muon spin precesses around wTF with a full asymmetry in a paramagnetic phase, whereas with a zero asymmetry in a magnetically ordered phase when the internal magnetic field is very large compared with wTF. The wTF asymmetry (A_{TF}) is therefore roughly proportional to the volume fraction of the paramagnetic phases in the sample. In fact, the wTF-μ^+SR spectrum exhibits a clear oscillation without relaxation at 60.5 K. Such amplitude, i.e., A_{TF} decreases with decreasing temperature from 43.4 K and becomes invisible at 39.3 K. Considering the presence of the precession signal due to the FM internal magnetic field in the early time domain below T_C (see Sec. III B), the wTF-μ^+SR spectrum was fitted in a time domain between 0.3 and 10 μs by a combination of an exponentially relaxing cosine oscillation due to wTF and an exponentially relaxing nonoscillatory signal formed by the FM tail component;

$$A_0 P_{TF}(t) = A_{TF} \cos(2\pi f_{TF} t + \phi_{TF}) \exp(-\lambda_{TF} t)$$
$$+ A_{tail} \exp(-\lambda_{tail} t), \quad (1)$$

where f_{TF} is the muon spin precession frequency due to wTF and is given by $f_{TF} = \gamma_\mu/2\pi \times 50\,\text{Oe} = 13.554\,\text{kHz/Oe} \times 50\,\text{Oe} \sim 0.68\,\text{MHz}$. The A_{tail} component corresponds to the signal from the magnetic ordered phase, in which the internal
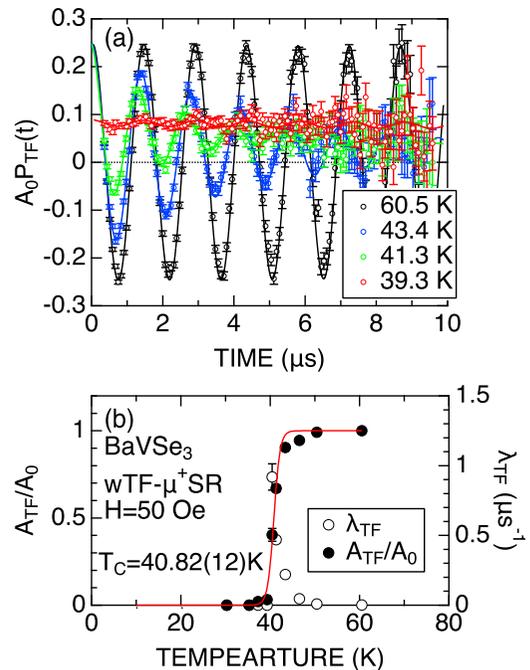
FIG. 3. (a) Weak transverse field (wTF)-μ^+SR spectra for BaVSe$_3$ recorded at selected temperatures and (b) the temperature dependencies of the asymmetry (A_{TF}) and exponential relaxation rate (λ_{TF}) originated from the precession signal by wTF. The magnitude of wTF was 50 Oe. In (a), solid lines represent the best fits with Eq. (2), and the data are shown in the time domain between 0.3 and 10 μs. In (b), a solid line represents the best fit with a Sigmoid function, and error bars are smaller than the data point symbols.

FM field is parallel to the initial muon spin polarization. Thus, the A_{tail} component appears only below T_C.

Figure 3(b) shows the temperature dependencies of the normalized wTF asymmetries (A_{TF}/A_0), where $A_0 = A_{TF}(60\,\text{K}) = 0.2455$, and the exponential relaxation rate (λ_{TF}) for the A_{TF} signal. As temperature decreases from 60 K, the $A_{TF}(T)/A_0$ curve exhibits a steplike decrease at around 40 K, while both A_{AF} and A_{tail} appear below 30 K. From the middle point of the steplike change in the $A_{TF}(T)/A_0$ curve, T_C and δT_C are determined as 40.82(12) K and 0.69(14) K, respectively, using a Sigmoid function. The $\lambda_{TF}(T)$ curve shows a clear maximum at around T_C, as a critical behavior of the magnetic transition. These results indicate that the sample is a single phase, i.e., no detectable impurity phase within the μ^+SR sensitivity, and the whole sample enters an FM phase below T_C.

B. ZF-μ^+SR at ambient pressure

Figure 4 shows the ZF-μ^+SR time spectrum for BaVSe$_3$ recorded at the lowest temperature measured (1.6 K). Since the spectrum exhibits a clear oscillation with almost full amplitude ($\sim$0.25), the whole volume of the sample is found to enter a FM ordered state. Furthermore, a complex time structure of the ZF spectrum indicates the presence of multiple components with different oscillatory frequencies. In fact, the Fourier transform of the time spectrum indicates the presence of two different frequency components [Fig. 4(b)], suggesting
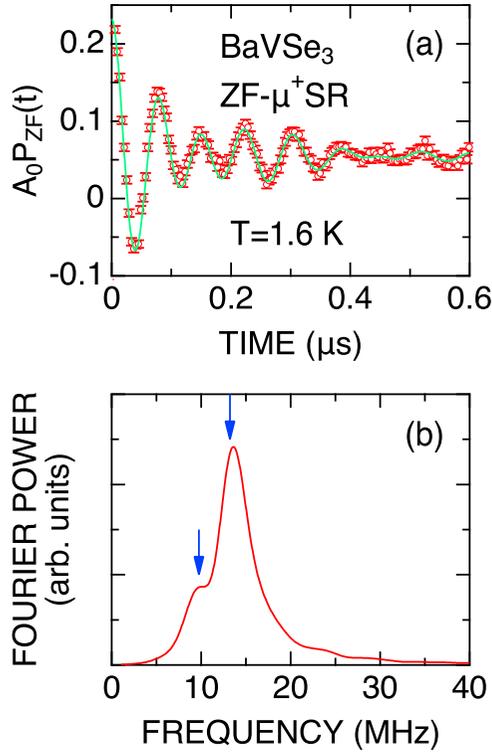
FIG. 4. (a) The zero field (ZF)-μ^+SR time spectrum for BaVSe$_3$ recorded at 1.6 K, and (b) the Fourier transform power spectrum of (a). In (a), a solid line represents a best fit with Eq. (2). In (b), two arrows represent the muon spin precession frequencies obtained by fitting the ZF-μ^+SR time spectrum with Eq. (2).

the existence of two magnetically different muon sites in the BaVSe$_3$ lattice.

Considering the internal magnetic field distribution in both a FM phase and a paramagnetic phase, the μ^+SR time spectrum was fitted by a combination of two exponentially relaxing cosine functions, an exponentially relaxing nonoscillatory signal for a $\frac{1}{3}$ tail signal in a powder sample [2,3], and a Gaussian Kubo-Toyabe signal for the sample in a paramagnetic state:

$$
\begin{aligned}
A_0 P_{ZF}(t) = {} & A_{FM1} \cos(2\pi f_{FM1} t) \exp(-\lambda_{FM1} t) \\
& + A_{FM2} \cos(2\pi f_{FM2} t) \exp(-\lambda_{FM2} t) \\
& + A_{tail} \exp(-\lambda_{tail} t) \\
& + A_{KT} G_{zz}^{KT},
\end{aligned} \tag{2}
$$

where A_0 is the initial asymmetry, A_{FM1}, A_{FM2}, A_{tail}, and A_{KT} are the asymmetries associated with the four signals, f_{FM1} and f_{FM2} are the muon Larmor frequencies corresponding to the quasistatic internal FM fields, λ_{FM1}, λ_{FM2}, and λ_{tail} are their exponential relaxation rates. Here, G_{zz}^{KT} is a static Gaussian Kubo-Toyabe function and given by [28]

$$
G_{zz}^{KT}(t, \Delta) = \tfrac{1}{3} + \tfrac{2}{3}(1 - \Delta^2 t^2) \exp\left(-\tfrac{1}{2}\Delta^2 t^2\right), \tag{3}
$$

where Δ is related to the width of the magnetic field distribution at the muon site in the paramagnetic state. To use the same fit function for the ZF-μ^+SR spectra in the whole temperature range, we have set $f_{FM1} = f_{FM2} = 0$ for $T \geqslant T_C$, and $A_{KT} = 0$
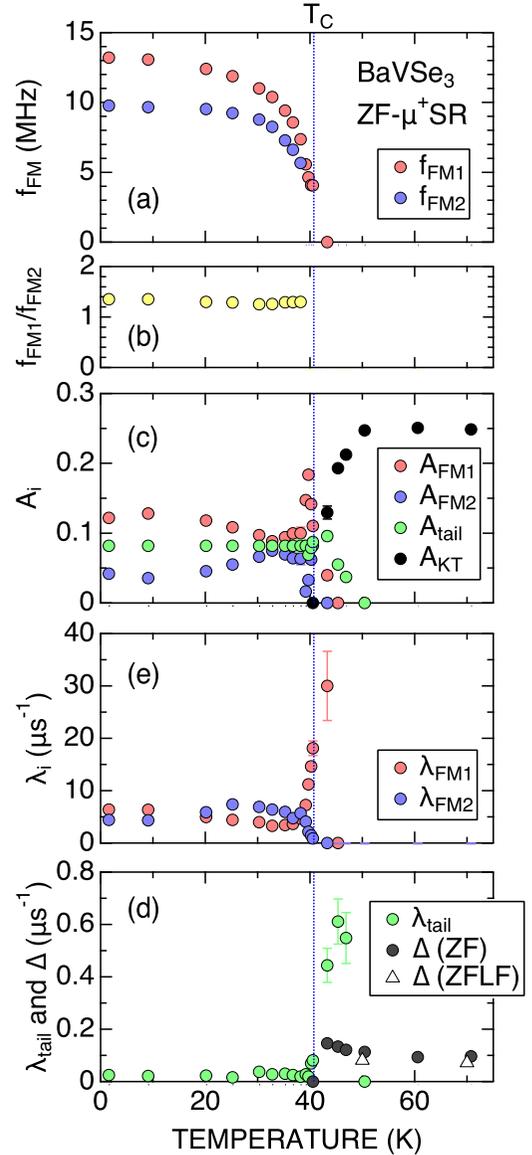
FIG. 5. The temperature dependencies of the zero field (ZF)-μ^+SR parameters in BaVSe$_3$ at ambient pressure. (a) The two muon spin precession frequencies (f_{FM1} and f_{FM2}), (b) the ratio between f_{FM1} and f_{FM2} (f_{FM1}/f_{FM2}), (c) the asymmetries (A_{FM1}, A_{FM2}, A_{tail}, and A_{KT}), (d) the exponential relaxation rates of A_{FM} signals (λ_{FM1} and λ_{FM2}), and (e) the exponential relaxation rate of the tail signal (λ_{tail}) and the field distribution width (Δ). The data were obtained by fitting the ZF-μ^+SR spectrum with Eqs. (2) and (3). Vertical broken lines show the Curie temperature determined by weak transverse field (wTF) measurements (see Fig. 3); that is, $T_C = 40.74(8)$ K . In (a) and (b), error bars are smaller than the data point symbols. In (d), Δ(ZFLF) represents Δ obtained by fitting the ZF- and longitudinal field (LF)-μ^+SR spectra simultaneously using a common Δ.

for $T < T_C$. Furthermore, below T_C, the asymmetries in the FM phase were fixed as follows: $(A_{FM1} + A_{FM2}) = \frac{2}{3}A_0$ and $A_{tail} = \frac{1}{3}A_0$, where $A_0 = 0.2455$ was estimated from the wTF-μ^+SR measurements at 60 K, which is well above T_C.

Figure 5 shows the temperature dependencies of the μ^+SR parameters in Eqs. (2) and (3). Each of the two precession frequencies (f_{FM1} and f_{FM2}) decreases with increasing

temperature and disappears at T_C. Below T_C, but above 39 K, the FM2 signal merges with the FM1 signal. The precession frequency-vs-temperature curve usually corresponds to the temperature dependence of the order parameter of a magnetic transition. In fact, since the ratio between the two oscillation frequencies ($f_{FM1}/f_{FM2} \sim 1.352$ at 1.6 K) is almost temperature independent up to below the vicinity of T_C, it is reasonable to assert that both f_{FM1} and f_{FM2} come from the internal magnetic field originated from the same FM phase in BaVSe$_3$ but from two unique magnetically different muon sites. Overall, the obtained result clearly indicates that the two oscillatory signals are not caused by the presence of multiple different magnetic phases in the sample, but are caused by the presence of multiple different muon sites in the BaVSe$_3$ lattice. Such an assertion is also supported by the wTF measurements presented above. In FM materials, the internal magnetic field at the muon site ($\boldsymbol{H}_\mu$) is not solely composed of dipolar fields ($\boldsymbol{H}_{dip}$) formed by FM ordered moments. This will be discussed in Sec. IV A.

As temperature increases from 2 K, A_{FM1} [A_{FM2}] slightly increases [decreases] up to about 10 K, then decreases [increases] up to about 30 K, and shows a complex temperature dependence around T_C. Although A_{tail} is fixed at $\frac{1}{3}A_0 = 0.08183$ up to about 40 K, A_{tail} decreases with further increasing temperature above T_C, and disappears around 50 K. Instead, A_{KT} increases with temperature above T_C and levels off to a maximum value at $T \geqslant 50$ K, meaning that the whole volume of the BaVSe$_3$ sample is in a paramagnetic state.

Both λ_{FM1} and λ_{FM2} are roughly temperature independent at $T < 35$ K. As temperature increases from 35 K, λ_{FM1} increases with temperature toward T_C and reaches a maximum slightly above T_C. On the contrary, λ_{FM2} gradually decreases with increasing temperature from 35 K, and disappears around T_C, since the FM2 signal merges into the FM1 signal.

For the tail signal, which corresponds to the parallel component of the internal magnetic fields with respect to the initial muon spin polarization, λ_{tail} is very small compared with λ_{FM} at temperatures below 40 K and is almost temperature independent. However, λ_{tail} increases with temperature close to T_C and reaches a maximum at around 43 K, like λ_{FM1}.

Since Δ is caused by nuclear magnetic moments of Ba, V, and Se, Δ is naturally negligible below T_C compared with a large FM field in the lattice. The value of Δ is around 0.1 μs^{-1}, which corresponds to about 1.2 Oe, and slightly decreases with temperature, as expected. Using the observed Δ (Δ^{obs}), the possible muon sites are further discussed in Sec. IV A.

C. μ^+SR at high pressures

For the μ^+SR measurements at high pressures, the BaVSe$_3$ discs with 6 mm diameter were set inside a pressure cell with an external diameter of about 26 mm. Hence, about 65% of the implanted muons stop in the pressure cell, and the rest (about 35%) stop in the sample. Since the pressure cell is paramagnetic even at the lowest temperature achievable on GPD, the muons stopped in the pressure cell provide an oscillatory signal due to wTF regardless of temperature. As a result, the normalized asymmetry [$A_{TF}(T)/A_0$] is unity at temperatures above T_C, while $A_{TF}(T)/A_0 \sim 0.65$ at temperatures
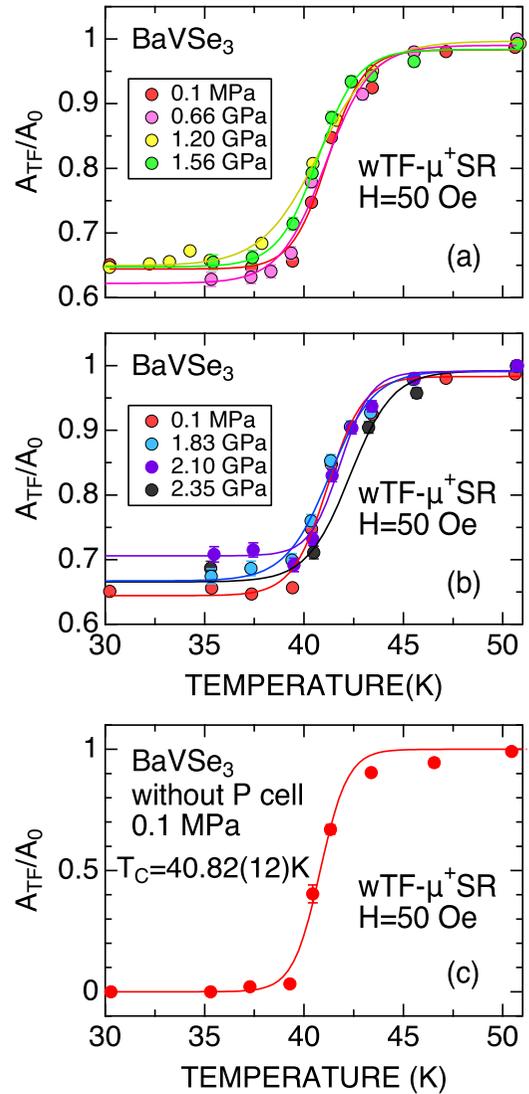
FIG. 6. The temperature dependence of the normalized A_{TF} (A_{TF}/A_0) recorded at several pressures obtained on GPD; (a) between 0.1 MPa and 1.56 GPa and (b) 0.1 MPa and between 1.83 and 2.35 GPa, and (c) 0.1 MPa, i.e., ambient pressure without pressure cell obtained on GPS [the same as Fig. 3(b)] for comparison. Solid lines represent the best fit with a Sigmoid function.

below T_C. Although the change in $A_{TF}(T)/A_0$ at T_C (~ 0.35) is smaller than that without pressure cell (~ 1), the wTF-μ^+SR measurements with temperature clearly provide T_C even in the pressure cell.

Figure 6 shows the temperature dependence of $A_{TF}(T)/A_0$ for several pressures together with the result obtained without the pressure cell in the same temperature range, for comparison. The wTF-μ^+SR spectrum in the pressure cell was also fitted by Eq. (2). At each pressure, the $A_{TF}(T)/A_0$ curve exhibits a steplike change at around 41 K, as in the case without the pressure cell [Fig. 6(c)]. From the middle point of the steplike change in the $A_{TF}(T)/A_0$ curve, T_C is estimated as 41.2(2) K at 0.1 MPa, which is roughly equivalent to the value estimated from the wTF data obtained without the pressure cell within the estimation accuracy [40.82(12) K]. As pressure
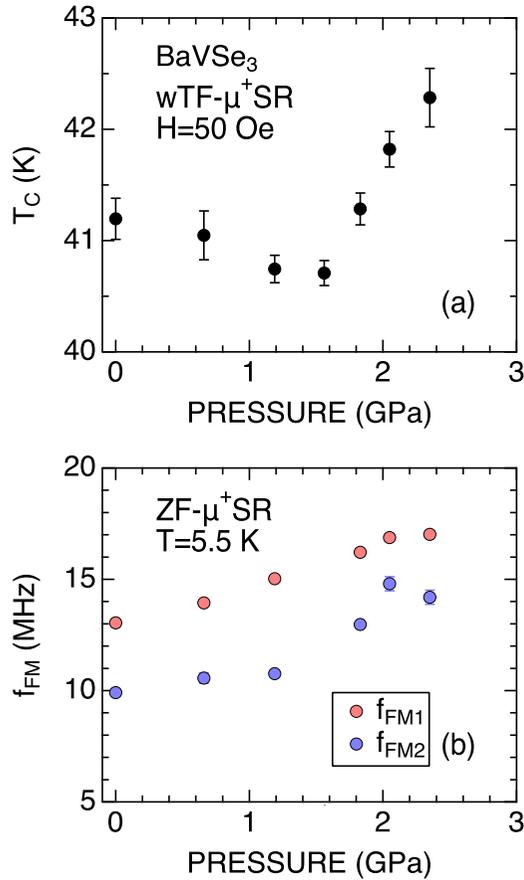
FIG. 7. The pressure dependence of (a) T_C and (b) the two muon spin precession frequencies at 5.5 K for BaVSe$_3$. The former data were obtained by fitting the $A_{TF}(T)/A_0$ curve with a Sigmoid function (see Fig. 6), and the latter data were obtained by fitting the zero field (ZF)-μ^+SR spectrum with Eq. (2).

(p) increases from 0.1 MPa to 1.56 GPa, T_C slightly shifts toward lower temperatures. Then T_C increases with further increasing p up to the highest pressure for this setup (2.35 GPa).

Using these $A_{TF}(T)/A_0$ curves, the estimated T_C is plotted as a function of p in Fig. 7(a). Here, T_C slightly decreases with pressure up to 1.56 GPa [$\delta T_C \equiv T_C(p) - T_C(0.1\,\text{MPa}) \sim -0.4\,\text{K}$ at $p = 1.56\,\text{GPa}$], then T_C starts to increase more rapidly with further increasing p ($\delta T_C \sim 1.1\,\text{K}$ at $p = 2.35\,\text{GPa}$). This behavior suggests the presence of two different interactions in BaVSe$_3$; one suppresses the formation of FM order, while the other enhances the formation of FM order. This is further discussed in Sec. IV.

Here, ZF-μ^+SR spectra for BaVSe$_3$ were recorded at 5.5 K at high pressures too. Such spectra were also fitted with Eq. (2), with a nonzero A_{KT} signal even below T_C. This is because the A_{KT} signal in this case corresponds to the signal from the muons stopped in the pressure cell and not the paramagnetic fraction of the sample. Figure 7(b) shows the p dependence of the two muon precession frequencies f_{FM1} and f_{FM2} at 5.5 K. Despite the complex p dependence of T_C, both f_{FM1} and f_{FM2} increase with p, suggesting the increase in the internal magnetic field at the muon sites. More precisely, f_{FM1} increases with p monotonically up to around 2 GPa and then

looks to level off to a constant value at around 17 MHz. On the contrary, f_{FM2} slowly increases with p up to around 1.5 GPa and then increases more rapidly with p up to 2.35 GPa. Considering the fact that $A_{FM1} > A_{FM2}$ below 10 K [see Fig. 5(b)], the $f_{FM1}(p)$ curve is more reliable than the $f_{FM2}(p)$ curve. Hence, the internal magnetic fields at the muon sites are found to increase monotonically with p.

IV. DISCUSSION

A. Internal magnetic field at ambient pressure

Before discussing the FM spin structure of BaVSe$_3$, the possible muon sites based on the μ^+SR result in the paramagnetic state is considered using the observed Δ (Δ^{obs}). Since the value of Δ at 0 K (Δ^{calc}) is predicted with the dipole field calculations (nuclear dipoles), the inequality $\Delta^{obs} \leqslant \Delta^{calc}$ is valid in the presence of any dynamics at nonzero temperatures. In fact, back to the related compound BaVS$_3$, $\Delta^{obs} = 0.725$ Oe at 43 K, while $\Delta^{calc} = 0.940$ Oe for the first site at $(\frac{2}{3}, \frac{1}{3}, \frac{3}{4})$ and 2.319 Oe for the second site at $(\frac{1}{3}, \frac{1}{3}, \frac{1}{2})$. Since the asymmetry of the signal from the first site is comparable with that from the second site [4], Δ^{obs} is found to be about a half of the prediction ($0.725 : \frac{0.940+2.319}{2} = 0.44 : 1$).

For BaVSe$_3$, $\Delta^{obs} = 0.1\,\mu s^{-1}$, which corresponds to 1.2 Oe, at 50 K [see Fig. 5(d)]. Hence, the scenario that the implanted muons locate only $\mu1$ ($\Delta^{calc} = 0.877$ Oe) and $\mu2$ ($\Delta^{calc} = 0.977$ Oe) is highly unlikely given the $\Delta^{obs} = 1.2$ Oe. If we assume a similar reduction of Δ^{obs} to that in BaVS$_3$, i.e., Δ^{obs} at 0 K is assumed to be about 2.4 Oe for BaVSe$_3$, a certain portion of the implanted muons should locate $\mu3$ ($\Delta^{calc} = 2.65$ Oe). This restricts the determination of the FM spin structure using the μ^+SR results.

For nonmagnetized FM materials in applied ZF, the internal magnetic field at a muon site (H_μ) is represented by [3,29–32]

$$H_{FM} = H_\mu$$
$$= H_{dip} + H_L + H_{hf}, \qquad (4)$$

where H_{dip} is the dipolar field, H_L is the Lorentz field, H_{hf} is the hyperfine field. Furthermore, H_L and H_{hf} are connected to the saturated magnetization (M_s) and the local spin density at the muon sites (ρ_{spin}) as follows:

$$H_{dip} = -\frac{1}{4\pi\mu_0}\nabla\left(\frac{m \cdot r}{r^3}\right),$$

$$H_L = \frac{4\pi}{3} \times M_s,$$

$$H_{hf} = \frac{8\pi}{3} \times \rho_{spin}(r_\mu) \times \frac{H_{dip}}{|H_{dip}|}. \qquad (5)$$

To estimate H_{dip}, we use the results of magnetization measurements for the magnitude and direction of the V moments. That is, the magnitude of the ordered V moment (M_V) is 0.34 μ_B along the c axis [19], which is equivalent to M_s at 2 K. Here, H_{dip} at the muon site is then easily calculated with DIPELEC [33] using the crystal structural data.

Assuming a FM ordering along the c axis ([0,0,FM]) with $M_V = M_{Vz} = 0.34\,\mu_B$, the predicted H_{dip}, H_L, and H_{hf} are summarized in Table I. It is very clear that the predicted

TABLE I. The predicted dipole field (H_{dip}), Lorentz field (H_L), hyperfine field (H_{hf}), total internal magnetic field (H_μ), corresponding muon spin precession frequency (f_μ), and field distribution width of a nuclear magnetic field (Δ^{calc}) at the three muon sites. The three muon sites predicted by DFT calculations are as follows: $\mu 1$ (0, 0.65, 0.75), $\mu 2$ (0, 0.56, 0.725), and $\mu 3$ (0.33, 0.67, 0). H_{dip} and Δ^{calc} were estimated by dipole field calculations with DIPELEC, H_L was calculated using Eq. (5) with $M_s = (0, 0, 0.34 \,\mu_B)$, i.e., $H_{L,z} = (4\pi/3)(N_A d/W_{\text{mw}})(0.34 \,\mu_B)$, where $N_A [= 6.022 \times 10^{23} \,(\text{mol}^{-1})]$ is the Avogadro's number, $d [= 5.55 \,(\text{g/cm}^3)]$ is the specific density, $W_{\text{mw}} [= 425.2 \,(\text{g/mol})]$ is the molar weight, and $1 \,\mu_B = 9.271 \times 10^{-21}$ erg/Oe. ρ_{spin} at each muon site was also predicted by DFT calculations as $-8.23212 \times 10^{-5} \,\mu_B/\text{Å}^3$ for $\mu 1$, $1.07134 \times 10^{-3} \,\mu_B/\text{Å}^3$ for $\mu 2$, and $-6.82441 \times 10^{-5} \,\mu_B/\text{Å}^3$ for $\mu 3$, when $M_{Vz} = 0.34 \,\mu_B$. Each component of H_{hf} was calculated using the relationship $H_{\text{hf}} = \frac{8\pi}{3}\rho(r_\mu)\frac{H_{\text{dip}}}{|H_{\text{dip}}|}$.

Magnetic structure x, y, z	μ^+ site	H_{dip} (Oe)	H_L (Oe)	H_{hf} (Oe)	H_μ (Oe)	f_μ[a] (MHz)	Δ^{calc}[b] (Oe)
[0,0,FM]	$\mu 1$	$(0, -14.6, -101.2)$	$(0, 0, 103.8)$	$(0, 0.9, 6.3)$	16.1	0.2	0.877
	$\mu 2$	$(0, 5.8, -98.5)$	$(0, 0, 103.8)$	$(0, 4.9, -83.1)$	78.8	1.1	0.977
	$\mu 3$	$(-17.0, -23.4, -290.3)$	$(0, 0, 103.8)$	$(0.3, 0.4, 5.3)$	183.7	2.5	2.65
[0,AF,FM]	$\mu 1$	$(0, -119.3, -176.0)$	$(0, 0, 103.8)$	$(0, 3.6, 5.3)$	133.8	1.8	0.877
	$\mu 2$	$(0, -51.7, -193.5)$	$(0, 0, 103.8)$	$(0, -21.5, -80.4)$	185.5	2.5	0.977
	$\mu 3$	$(642.7, 519.5, -527.1)$	$(0, 0, 103.8)$	$(-3.5, -2.8, 2.9)$	923.4	12.5	2.65
[AF,0,FM]	$\mu 1$	$(305.6, -16.0, -111.4)$	$(0, 0, 103.8)$	$(-6.0, 0.3, 2.2)$	300.0	4.1	0.877
	$\mu 2$	$(437.1, 6.3, -108.5)$	$(0, 0, 103.8)$	$(80.8, 1.2, -20.1)$	518.5	7.0	0.977
	$\mu 31$	$(-51.0, 487.1, -337.7)$	$(0, 0, 103.8)$	$(0.5, -4.3, 3.0)$	537.6	7.3	2.65
	$\mu 32$	$(-14.0, 537.7, -301.0)$	$(0, 0, 103.8)$	$(0.1, -4.6, 2.6)$	567.7	7.7	2.65
[AF,AF,FM]	$\mu 1$	$(414.7, -109.8, -161.9)$	$(0, 0, 103.8)$	$(-5.8, 1.5, 2.3)$	426.7	5.8	0.877
	$\mu 2$	$(593.2, -47.6, -178.1)$	$(0, 0, 103.8)$	$(79.5, -6.4, -23.9)$	682.0	9.2	0.977
	$\mu 31$	$(546.6, 1172.3, -509.0)$	$(0, 0, 103.8)$	$(-2.1, -4.5, 1.9)$	1350.3	18.3	2.65
	$\mu 32$	$(-634.5, 217.1, -459.7)$	$(0, 0, 103.8)$	$(4.1, -1.4, 3.0)$	754.1	10.2	2.65

[a]The observed f_μs are $f_{\text{FM1}} = 13.21(4)$ MHz and $f_{\text{FM2}} = 9.94(6)$ MHz at 1.6 K.
[b]The observed Δ (Δ^{obs}) is 1.2 Oe at 50 K.

internal magnetic field (H_μ) at each muon site is too small to explain the experimental result. If we further assume $M_V = M_{Vz} = 0.6(2) \,\mu_B$ based on the magnetization measurements for a single crystal sample [20], the predicted H_μ (f_μ) are still too small to explain the experimental result [see Fig. 8(a)]. In fact, the predicted $f_{\mu 1}$ and $f_{\mu 2}$ are about 6% and 16% of the measured f_{FM2} at 1.6 K even if $M_{Vz} = 1 \,\mu_B$, although $f_{\mu 3}$ is about 60% of f_{FM1} at 1.6 K.

Therefore, we have attempted to introduce an AF component in the ab plane so as to avoid geometrical frustration. Here, the ordered V moment (M_V) is represented by (M_{Vx}, M_{Vy}, M_{Vz}). Back to Fig. 1, [0,AF,FM] means that V moments align parallel along the b axis but antiparallel between the neighboring V ions along the c axis, while [AF,0,FM] means that V moments align parallel along the a axis but antiparallel between the neighboring V ions along the b axis. For both [0,AF,FM] and [AF,0,FM], V moments align parallel along the c axis. Here, [AF,AF,FM] is a combination of [0,AF,FM] and [AF,0,FM]. The direction and magnitude of M_V are [011] and [0$\bar{1}$1] for [0,AF,FM], [101] and [$\bar{1}$01] for [AF,0,FM], and [111] and [$\bar{1}\bar{1}$1] for [AF,AF,FM] with $M_{Vz} = 0.34 \,\mu_B$. More correctly, $(M_{Vx}, M_{Vy}, M_{Vz}) = (0, 0.70, 0.34) \,\mu_B$ for [011], and $(0.41, 0.70, 0.34) \,\mu_B$ for [111], because $a = 6.992(2)$Å, $b = 12.113(3)$Å, and $c = 5.859(1)$Å [17]. The canting angle of the ordered V moments for [0,AF,FM] is 64° along the b axis (α), for [AF,0,FM] is 50° along the a axis (β), and for [AF,AF,FM] is 67° along the [110] direction. Furthermore, for [AF,0,FM] and [AF,AF,FM], the μ_3 site is no longer magnetically equivalent, but splits into two magnetically different sites ($\mu 31$ and $\mu 32$). That

is, among the eight equivalent μ_3 sites per unit cell in a paramagnetic state, four sites become the $\mu 31$ site, and the rest become the $\mu 32$ site below T_C.

Figures 8(b)–8(d) show the relationship between M_{Vz} and the predicted internal magnetic field (H_μ and f_μ) for [0,AF,FM], [AF,0,FM], and [AF,AF,FM]. The [0,AF,FM] model is clearly excluded because both $f_{\mu 1}$ and $f_{\mu 2}$ are too small to explain f_{FM2} in the whole M_{Vz} range between 0 and $1.1 \,\mu_B$. Considering the fact that $A_{\text{FM1}} > A_{\text{AF2}}$ [see Fig. 5(b)], the [AF,AF,FM] model is also excluded. This is because the population of the muons at the $\mu 31$ site is the same to that at the $\mu 32$ site, resulting in $A_{\text{FM1}} = A_{\text{AF2}}$. When the muons at the $\mu 2$ site also contribute to the lower f_μ signal, i.e., the f_{FM2} signal, $A_{\text{FM1}} < A_{\text{AF2}}$, being inconsistent with the experimental result.

To reproduce the ratio between f_{FM1} and f_{FM2}, Fig. 9(a) shows the relationship between $f_{\mu 3}$ and $f_{\mu 2}$, i.e., $\frac{f_{\mu 31}+f_{\mu 32}}{2f_{\mu 2}}$ and the canting angle toward the a axis (β) for [AF,0,FM]. As M_{Vz} increases from 0.34 to $1.13 \,\mu_B$, the intersection between the $\frac{f_{\mu 31}+f_{\mu 32}}{2f_{\mu 2}}(\beta)$ curve and the observed $f_{\text{FM1}}/f_{\text{FM2}}(=1.352)$ shifts toward a higher β side. Moreover, when $f_{\mu 3}/f_{\mu 2} = 1.352$, the predicted $f_{\mu 2}$ increases monotonically with M_{Vz}, as seen in Fig. 9(c). To explain the observed $f_{\text{FM2}}(= 9.75 \text{ MHz})$ and $f_{\text{FM1}}/f_{\text{FM2}}(=1.352)$, we obtain that $\beta = 28°$ and $M_{Vz} = 1.11 \,\mu_B$ ($M_{Vx} = 0.59 \,\mu_B$), which is comparable with the magnetization measurement results for a single-crystal sample $[M_{Vz} = 0.6(2) \,\mu_B]$ [20] and the previous DFT calculation results ($M_{Vz} = 0.82 \,\mu_B$) [21]. The total ordered moment is thus obtained as $M_V = \sqrt{M_{Vx}^2 + M_{Vz}^2} = 1.26 \,\mu_B$.
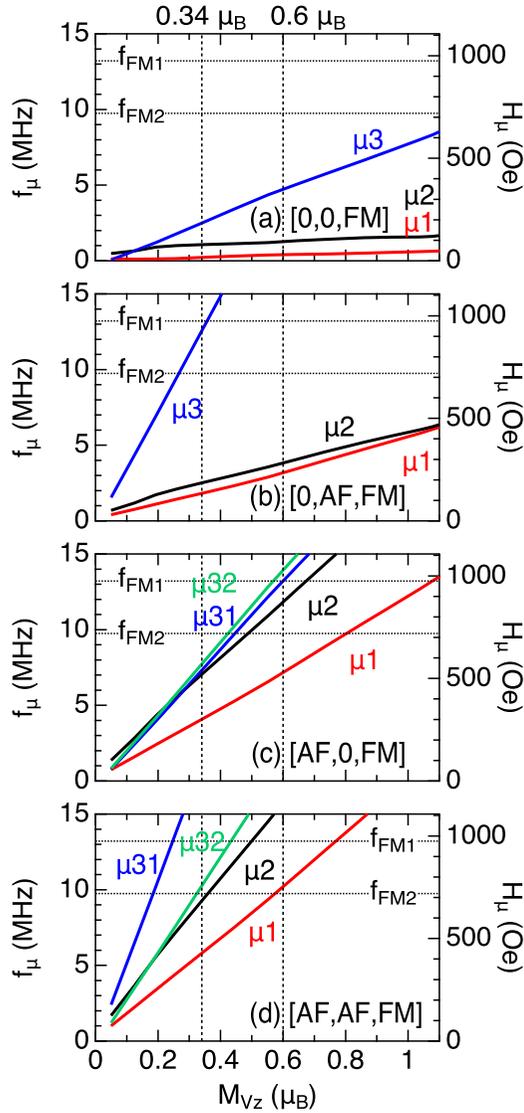
FIG. 8. The relationship between the magnitude of the ordered V moment along the c axis (M_{Vz}) and the predicted internal magnetic field (H_μ and f_μ) at the three muon sites for the ferromagnetic (FM) order (a) along the c axis ([0,0,FM]), (b) along the c axis but antiferromagnetic (AF) along the b axis ([0,AF,FM]), (c) along the c axis but AF along the a axis ([AF,0,FM]), and (d) along the c axis but AF along the a and b axes ([AF,AF,FM]). f_{FM1} and f_{FM2} correspond to the measured values obtained at 1.6 K. Here, we assumed that $M_{sz} = M_{Vz}$. Two vertical broken lines show the previously reported $M_{Vz}(= 0.32\,\mu_B$ and $0.6\,\mu_B)$ by magnetization measurements [19,20].

FIG. 9. The relationship between $f_{\mu3}/f_{\mu2}$ and the canting angle for (a) the [AF,0,FM] model and (b) the [0,AF,FM] model. In (a), the ordered V moment along the c axis (M_{Vz}) is changed from 0.34 to $1.13\,\mu_B$, $f_{\mu3}/f_{\mu2} = \frac{f_{\mu31}+f_{\mu32}}{2f_{\mu2}}$, and the canting angle toward the a axis (β). In (b), M_{Vz} is changed from 0.05 to $0.34\,\mu_B$ and the canting angle toward the b axis (α). (c) $f_{\mu2}$ as a function of M_{Vz}, when $f_{\mu3}/f_{\mu2} = 1.352$. For [0,AF,FM], only $M_{Vz} \leqslant 0.19\,\mu_B$ satisfies $f_{\mu3}/f_{\mu2} = 1.352$.

On the contrary, for the [0,AF,FM] model, the intersection between the $\frac{f_{\mu3}}{f_{\mu2}}(\alpha)$ curve and the observed $f_{FM1}/f_{FM2}(=1.352)$ exists only when $M_{Vz} \leqslant 0.19\,\mu_B$ [see Fig. 9(b)]. As a result, the predicted $f_{\mu2}$ ranges below 1 MHz, which is too small to explain the observed $f_{FM2}(=9.75\,\text{MHz})$. Therefore, the FM spin structure is uniquely determined from the present μ^+SR result. To further confirm the present proposed FM spin structure, it is highly preferable to measure neutron diffraction due to its unique power for determining periodic magnetic structures.

B. Internal magnetic field at high pressures

Comparing with the previous μ^+SR work on an incommensurate AF (IC-AF) BaVS$_3$ (Fig. 10) [4], the distribution of the internal magnetic field in BaVSe$_3$ is like that in BaVS$_3$, except for the broad maximum around 20 MHz in BaVS$_3$ due to a wide field distribution caused by the IC-AF order [2–4,34]. This also supports that the FM spin structure of BaVSe$_3$ is not a simple [0,0,FM] but a canted [AF,0,FM]. Note that, in BaVS$_3$, the exchange interaction along the chain direction, i.e., the c axis, (J_{ex}^c) is known to be FM and very strong compared with the AF interchain (in plane) exchange interactions (J_{ex}^{ab}) [35]. Nevertheless, relatively weak J_{ex}^{ab} plays
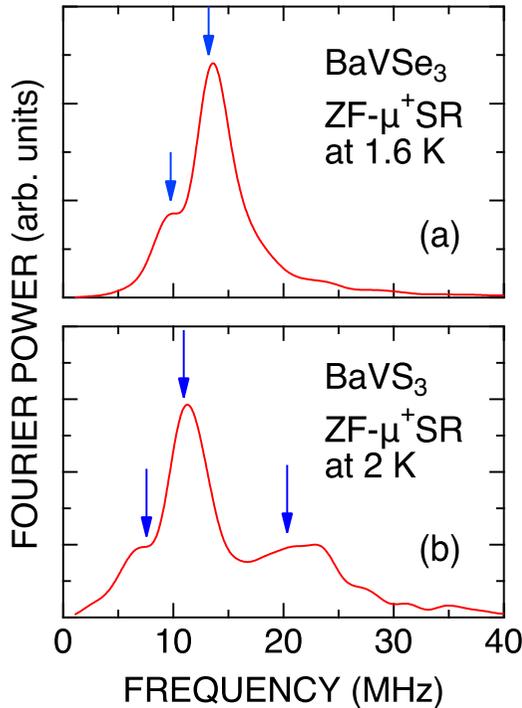
FIG. 10. The Fourier transform power frequency spectrum of the zero field (ZF)-μ^+SR spectrum for (a) BaVSe$_3$ and (b) BaVS$_3$ [4]. The ZF-μ^+SR spectra for BaVSe$_3$ (BaVS$_3$) was recorded at 1.6 K (2.0 K) without the pressure cell. (a) The same as Fig. 4(b). Arrows represent the frequencies to fit the ZF-μ^+SR spectrum (see text and Ref. [4]). In (b), the broad maximum around 20 MHz comes from a wide field distribution in BaVS$_3$ caused by incommensurate antiferromagnetic (IC-AF) order.

a significant role in forming the IC-AF ground state. For other Q1D compounds with FM-J_{ex}^c, the magnetic ground states depend on J_{ex}^{ab}, such as a modulated AF ordered state for BaCoO$_3$ [36] and a helical AF ordered state for CsCuCl$_3$ [37].

Before discussing the complex pressure dependence of T_C found with high-pressure μ^+SR [Fig. 7(a)], a first question to answer is why BaVSe$_3$ enters an FM phase at low temperatures, while BaVS$_3$ enters an AF phase. The structural phase transition at $T_s = 310$ K from a hexagonal phase to a noncentrosymmetric orthorhombic phase with $Cmc2_a$ space group could allow a Dzyaloshinski-Moriya (DM) interaction [38–40] between the 1D chains in the orthorhombic phase of BaVSe$_3$ due to the distortion of both the 1D chain and 2DTL, as in the case for CsCuCl$_3$ [41]. The presence of the DM interaction is also reported for NaV$_2$O$_5$ [42,43] and Sr$_2$V$_3$O$_9$ [44,45]. This could lead to the formation of weak ferromagnetism below T_C. The M-H curve shown in Fig. 2(b) is also consistent with a weak ferromagnetism.

Note that BaVS$_3$ also enters the orthorhombic phase with either $Cmcm$ [9] or $Cmc2_1$ [46] space group below $T_s = 250$ K. The former is centrosymmetric, while the latter lacks centrosymmetry as well as $Cmc2_a$ for BaVSe$_3$. Furthermore, BaVS$_3$ exhibits a metal-to-insulator transition at $T_{MI} = 70$ K accompanying a doubling of the unit cell along the c axis [5–7,47]. Such a transition is induced by Peierls instability

of V^{4+} ions, which leads to the formation of CDW order [9,10,47]. As a result, the DM interaction is thought to be suppressed in BaVS$_3$, and the IC-AF ordered state is stabilized as a magnetic ground state [4,11].

Back to BaVSe$_3$, the p dependence of T_C clearly indicates the presence of two different exchange interactions in the ab plane; i.e., one decreases T_C with p, whereas the other increases T_C with p. The former interaction is predominant up to around 1.5 GPa, while the latter overcomes the former at $p > 1.5$ GPa. The former interaction naturally corresponds to J_{ex}^{ab} and the latter corresponds to the DM interaction. Since the interchain distance on the 2DTL decreases with increasing p, J_{ex}^{ab} would be also enhanced with p. However, as p further increases above 1.5 GPa, the noncentrosymmetric distortion is likely to be enhanced with p, leading to the increase in the DM interaction. On the contrary, J_{ex}^c is also expected to be enhanced with p through the decrease in the distance between the neighboring V ions in the chain, while such an enhancement is most unlikely essential for forming long-rang magnetic order *via* the interchain interactions. To further elucidate the role of each interaction, we will need to study the crystal structure and magnetic anisotropy under p using a single-crystal sample.

V. SUMMARY

We have investigated the microscopic magnetic nature of BaVSe$_3$ at ambient and high pressures with μ^+SR using a powder sample. The μ^+SR measurements in a ZF at ambient pressure clarified the appearance of a clear oscillatory signal below $T_C \sim 41$ K, which evidenced the formation of static FM order. Analyzing the internal magnetic field, it was suggested that the FM spin structure is not a simple one with an easy magnetization axis along the c axis. The detailed analysis of the internal magnetic field suggested that the V moments align FM along the c axis but slightly canted toward the a axis by 28° that is coupled AF, namely, the ordered V moment (M_V) is (0.59, 0, 1.11) μ_B.

The μ^+SR measurements in a wTF at high pressures showed that T_C slightly decreases with pressure (p) up to 1.5 GPa, then T_C increases rapidly with p for $p > 1.5$ GPa. This suggested the presence of the two magnetic interactions in the ab plane: one is an AF interaction, and the other is an FM interaction. The former is enhanced with p up to 1.5 GPa, although the latter is predominant at $p > 1.5$ GPa.

[1] M. E. Zhitomirsky, O. A. Petrenko, and L. A. Prozorova, Phys. Rev. B **52**, 3511 (1995).

[2] G. M. Kalvius, D. R. Noakes, and O. Hartmann, *Handbook on the Physics and Chemistry of Rare Earths* (North-Holland, Amsterdam, 2001), Vol. 32, Chap. 206, pp. 55–451.

[3] A. Yaouanc and P. D. de Réotier, *Muon Spin Rotation, Relaxation, and Resonance, Application to Condensed Matter* (Oxford, New York, 2011).

[4] J. Sugiyama, D. Andreica, O. K. Forslund, E. Nocerino, N. Matsubara, Y. Sassa, Z. Guguchia, R. Khasanov, F. L. Pratt, H. Nakamura, and M. Månsson, Phys. Rev. B **101**, 174403 (2020).

[5] R. A. Gardner, M. Vlasse, and A. Wold, Acta Crystallogr. Sect. B **25**, 781 (1969).

[6] M. Takano, H. Kosugi, N. Nakanishi, M. Shimada, T. Wada, and M. Koizumi, J. Phys. Soc. Jpn. **43**, 1101 (1977).

[7] O. Massenet, J. Since, J. Mercier, M. Avignon, R. Buder, V. Nguyen, and J. Kelber, J. Phys. Chem. Solids **40**, 573 (1979).

[8] H. Imai, H. Wada, and M. Shiga, J. Phys. Soc. Jpn. **65**, 3460 (1996).

[9] T. Inami, K. Ohwada, H. Kimura, M. Watanabe, Y. Noda, H. Nakamura, T. Yamasaki, M. Shiga, N. Ikeda, and Y. Murakami, Phys. Rev. B **66**, 073108 (2002).

[10] S. Fagot, P. Foury-Leylekian, S. Ravy, J.-P. Pouget, and H. Berger, Phys. Rev. Lett. **90**, 196401 (2003).

[11] H. Nakamura, T. Yamasaki, S. Giri, H. Imai, M. Shiga, K. Kojima, M. Nishi, K. Kakurai, and N. Metoki, J. Phys. Soc. Jpn. **69**, 2763 (2000).

[12] T. Graf, D. Mandrus, J. M. Lawrence, J. D. Thompson, P. C. Canfield, S.-W. Cheong, and L. W. Rupp, Phys. Rev. B **51**, 2037 (1995).

[13] L. Forró, R. Gaál, H. Berger, P. Fazekas, K. Penc, I. Kézsmárki, and G. Mihály, Phys. Rev. Lett. **85**, 1938 (2000).

[14] I. Kézsmárki, G. Mihály, R. Gaál, N. Barišić, H. Berger, L. Forró, C. C. Homes, and L. Mihály, Phys. Rev. B **71**, 193103 (2005).

[15] S. Bernu, P. Fertey, J.-P. Itié, H. Berger, P. Foury-Leylekian, and J.-P. Pouget, Phys. Rev. B **86**, 235105 (2012).

[16] K. Momma and F. Izumi, J. Appl. Cryst. **44**, 1272 (2011).

[17] N. J. Poulsen, Mater. Res. Bull. **33**, 313 (1998).

[18] J. Kelber, A. Reis, A. Aldred, M. Mueller, O. Massenet, G. DePasquali, and G. Stucky, J. Solid State Chem. **30**, 357 (1979).

[19] T. Yamasaki, S. Giri, H. Nakamura, and M. Shiga, J. Phys. Soc. Jpn. **70**, 1768 (2001).

[20] M. Herak, M. Miljak, A. Akrap, L. Forro, and H. Berger, J. Phys. Soc. Jpn. **77**, 093701 (2008).

[21] A. Akrap, V. Stevanović, M. Herak, M. Miljak, N. Barišić, H. Berger, and L. Forró, Phys. Rev. B **78**, 235111 (2008).

[22] D. Grieger, L. Boehnke, and F. Lechermann, J. Phys.: Condens. Matter **22**, 275601 (2010).

[23] Z. Shermadini, R. Khasanov, M. Elender, G. Simutis, Z. Guguchia, K. Kamenev, and A. Amato, High Press. Res. **37**, 449 (2017).

[24] R. Khasanov, Z. Guguchia, A. Maisuradze, D. Andreica, M. Elender, A. Raselli, Z. Shermadini, T. Goko, F. Knecht, E. Morenzoni, and A. Amato, High Press. Res. **36**, 140 (2016).

[25] O. K. Forslund, D. Andreica, Y. Sassa, H. Nozaki, I. Umegaki, E. Nocerino, V. Jonsson, O. Tjernberg, Z. Guguchia, Z. Shermadini, R. Khasanov, M. Isobe, H. Takagi, Y. Ueda, J. Sugiyama, and M. Månsson, Sci. Rep. **9**, 1141 (2019).

[26] A. Suter and B. Wojek, Phys. Procedia **30**, 69 (2012).

[27] P. Blaha, K. Schwarz, F. Tran, R. Laskowski, G. K. H. Madsen, and L. D. Marks, J. Chem. Phys. **152**, 074101 (2020).

[28] R. Kubo and T. Toyabe, *Magnetic Resonance and Relaxation* (North-Holland, Amsterdam, 1996).

[29] S. Barth, E. Albert, G. Heiduk, A. Möslang, A. Weidinger, E. Recknagel, and K. H. J. Buschow, Phys. Rev. B **33**, 430 (1986).

[30] A. Schenck and F. N. Gygax, *Handbook of Magnetic Materials* (Elsevier, Amsterdam, 1995), Vol. 9, Chap. 2.

[31] J. Sugiyama, H. Nozaki, M. Månsson, K. Prša, D. Andreica, A. Amato, M. Isobe, and Y. Ueda, Phys. Rev. B **85**, 214407 (2012).

[32] J. Sugiyama, K. Miwa, H. Nozaki, Y. Kaneko, B. Hitti, D. Arseneau, G. D. Morris, E. J. Ansaldo, and J. H. Brewer, Phys. Rev. Mater. **3**, 064402 (2019).

[33] K. M. Kojima, J. Yamanobe, H. Eisaki, S. Uchida, Y. Fudamoto, I. M. Gat, M. I. Larkin, A. Savici, Y. J. Uemura, P. P. Kyriakou, M. T. Rovers, and G. M. Luke, Phys. Rev. B **70**, 094402 (2004).

[34] D. Andreica, Ph.D. thesis, ETH Zurich, 2001.

[35] X. Jiang and G. Y. Guo, Phys. Rev. B **70**, 035110 (2004).

[36] H. Nozaki, M. Janoschek, B. Roessli, J. Sugiyama, L. Keller, J. H. Brewer, E. J. Ansaldo, G. D. Morris, T. Takami, and H. Ikuta, Phys. Rev. B **76**, 014402 (2007).

[37] K. Adachi, N. Achiwa, and M. Mekata, J. Phys. Soc. Jpn. **49**, 545 (1980).

[38] I. Dzyaloshinsky, J. Phys. Chem. Solids **4**, 241 (1958).

[39] T. Moriya, Phys. Rev. **117**, 635 (1960).

[40] T. Moriya, Phys. Rev. **120**, 91 (1960).

[41] A. Sera, Y. Kousaka, J. Akimitsu, M. Sera, T. Kawamata, Y. Koike, and K. Inoue, Phys. Rev. B **94**, 214408 (2016).

[42] H. Nojiri, S. Luther, M. Motokawa, M. Isobe, and Y. Ueda, J. Phys. Soc. Jpn. **69**, 2291 (2000).

[43] T. Rõõm, D. Hüvonen, U. Nagel, Y.-J. Wang, and R. K. Kremer, Phys. Rev. B **69**, 144410 (2004).

[44] V. A. Ivanshin, V. Yushankhai, J. Sichelschmidt, D. V. Zakharov, E. E. Kaul, and C. Geibel, Phys. Rev. B **68**, 064404 (2003).

[45] A. Rodríguez-Fortea, M. Llunell, P. Alemany, and E. Canadell, Phys. Rev. B **82**, 134416 (2010).

[46] M. Ghedira, M. Anne, J. Chenavas, M. Marezio, and F. Sayetat, J. Phys. C: Solid State Phys. **19**, 6489 (1986).

[47] P. Foury-Leylekian, P. Leininger, V. Ilakovac, Y. Joly, S. Bernu, S. Fagot, and J.-P. Pouget, Physica B Condens. Matter **407**, 1692 (2012).